ELSEVIER

Journal of Molecular Catalysis A: Chemical 126 (1997) 169-184

JOURNAL OF MOLECULAR CATALYSIS A: CHEMICAL

Effect of the addition of chromium- and manganese oxides on structural and catalytic properties of copper/zirconia catalysts for the synthesis of methanol from carbon dioxide

M. Kilo [a,1], J. Weigel [b], A. Wokaun [b,c], R.A. Koeppel [c], A. Stoeckli [c], A. Baiker [c,*]

[a] *Physical Chemistry II, University of Bayreuth, D-95440 Bayreuth, Germany*
[b] *Paul Scherrer Institute, CH-5232 Villigen, Switzerland*
[c] *Department of Chemical Engineering and Industrial Chemistry, Swiss Federal Institute of Technology, ETH Zentrum, CH-8092 Zurich, Switzerland*

Received 15 April 1997; accepted 19 May 1997

Abstract

The effect of chromium- and manganese oxide on the structural and catalytic properties of copper/zirconia used for methanol synthesis from carbon dioxide and hydrogen has been investigated by several techniques (TG/DTA, XRD, TPR, XPS, N_2O-titration, nitrogen physisorption). The methanol selectivity of all catalysts is governed by the competition of the simultaneously catalyzed methanol synthesis and reverse water gas shift reaction. The chromium containing sample produces predominantly methanol, whereas the manganese containing catalyst is most active for CO formation. For reaction temperatures 443–513 K and 1.7 MPa total pressure, methanol formation decreases in the order $Cu/ZrO_2 > Cu/CrO_x/ZrO_2 > Cu/MnO_x/ZrO_2$ for catalysts dried at 403 K. After calcination at 623 K in air, methanol synthesis activity is similar for all catalysts. For temperatures exceeding 523 K $Cu/CrO_x/ZrO_2$ shows highest activity for methanol production. The addition of chromium oxide and less pronounced manganese oxide, to Cu/ZrO_2 retards sintering of the copper component and shifts the crystallization of amorphous zirconia to higher temperatures, thus, resulting in an increased thermal stability of the catalyst under reaction conditions. X-ray photoelectron spectroscopy (XPS) was applied to examine the relative surface concentrations and the oxidation state of the catalyst components. XPS shows that there is no apparent correlation between the oxidation states of the metals and the catalytic properties of the catalysts. In situ diffuse reflectance FTIR studies were performed to identify the species present on the catalyst surface under CO_2 hydrogenation conditions and to elucidate the reaction mechanism. With all catalysts, surface carbonate and formate species were formed rapidly. Evidence is given that over copper/zirconia based catalysts methanol is formed mainly from bidentate surface carbonate via adsorbed CO, π-bound formaldehyde and surface-bound methylate. © 1997 Elsevier Science B.V.

Keywords: Carbon dioxide hydrogenation; Methanol synthesis; Copper/zirconia; Chromium oxide promotion; Manganese oxide promotion; Catalyst characterization

1. Introduction

The synthesis of methanol from $CO/CO_2/H_2$ mixtures is a well established industrial

* Corresponding author. Tel.: +41-1-6323153; fax: +41-1-6321163; e-mail: baiker@tech.chem.ethz.ch

[1] Present address: Institut für Allgemeine Metallurgie, TU Clausthal, D-38678 Clausthal-Zellerfeld.

PII S1381-1169(97)00109-X

process [1,2]. The catalysts most frequently used contain copper as active component, zinc oxide and alumina or chromium oxide as a structural promoter. In the past few years, several metal oxides have been tested as alternative support materials for CO/CO_2 hydrogenation catalysts. Among these materials, ZrO_2 is of special interest because of its mechanical and thermal stability, its high specific surface area and its intrinsic catalytic properties [3–7]. Pure ZrO_2 shows distinct activity and selectivity for methanol synthesis at higher temperature.

Although methanol synthesis is a well established industrial process and extensive research has been performed on this subject [1,2,8], there still exists much controversy regarding some fundamental aspects of the reaction. For commercial methanol synthesis catalysts it has been proposed that methanol is formed from CO_2 [9], whereby the support plays a minor role [10]. Moreover, it was found that under synthesis conditions the copper surface is partially oxidized, with the extent of the oxidation depending on the CO/CO_2 ratio in the feedstock [11,12]. In contrast, on zirconia supported catalysts the importance of the support has been emphasized by several authors [5,6,13] and the crucial role of the metal–zirconia interface in methanol synthesis has been discussed [14,15]. It appears likely that on the reaction path from CO_2 to CH_3OH several reaction steps take place on the support, whereas others proceed on the metallic component.

The effect of the addition of oxides such as MnO_x or CrO_x to Cu/ZnO based methanol synthesis catalysts has been reported in several articles [2,16–21]. The components are added in order to stabilize the catalyst against sintering, to effect the catalytic behavior, or to alter the structural properties of the resulting materials as well as the degree of the Cu–ZnO interaction. Kotowski et al. [18] showed that the addition of Mn to a Cu/ZnO catalyst increased the rate of methanol production. Other authors reported that the addition of MnO or Cr_2O_3 favors the formation of higher alcohols [16,17,19–21]. By investigating $CuO–ZnO–Cr_2O_3$ catalysts for CO hydrogenation, Campos-Martín et al. [16] proposed that chromia acts as a structural promotor which retards sintering of the copper by thermal effects but does not participate in the catalytic sites. A similar thermo-stabilizing effect of chromia was reported by other authors [17,19], whereas Chen et al. [22] discussed the origin of the promotion ability of Cr_2O_3 on copper catalysts for CO hydrogenation on the basis of an electronic interaction model.

The aim of the present study was to investigate the effect of chromium and manganese oxide on the structural and catalytic properties of copper/zirconia catalysts for methanol synthesis from carbon dioxide and hydrogen. Catalysts prepared by sequential precipitation were characterized by means of nitrogen adsorption, thermal analysis (TG/DTA), X-ray diffraction (XRD), temperature-programmed reduction (TPR) and N_2O-titration. XPS measurements have been carried out to elucidate the changes of the surface during pretreatment and reaction with CO_2/H_2 mixtures. In addition, the surface intermediates prevailing on the catalysts during CO and CO_2 hydrogenation were studied by in situ FTIR spectroscopy.

2. Experimental

2.1. Catalysts

The catalysts investigated were prepared by sequential precipitation of the corresponding metal nitrates at constant pH (pH 7) and constant temperature (363–368 K). Binary Cu/ZrO_2 (30 at% Cu/70 at% Zr) was obtained by simultaneously adding aqueous solutions of $ZrO(NO_3)_2$ and NaOH at pH 7 to a Pyrex vessel containing deionized water. After 5 min ageing under stirring, aqueous solutions of $Cu(NO_3)_2 \cdot 3H_2O$ and NaOH were added simultaneously at pH 7. The resulting voluminous dark brown gel was aged for 15 min, cooled to room temperature, filtered using a glass filter and thoroughly washed with deionized water.

After drying in vacuo for 15 h at 403 K, the sample was crushed to a grain size of 50–150 μm. Calcination was performed for 3 h in static air at 623 K. Ternary samples containing Mn or Cr (30 at% Cu/14 at% Mn, Cr/56 at% Zr) were prepared similarly by first precipitating the Zr component together with the Mn ($Mn(NO_3)_2 \cdot 4H_2O$) or Cr ($Cr(NO_3)_3 \cdot 9H_2O$) constituent, respectively. All chemicals used were of analytical grade. Throughout the work, acronyms are used for the catalysts, i.e. Zr for Cu/ZrO_2, CrZr for $Cu/CrO_x/ZrO_2$ and MnZr for $Cu/MnO_x/ZrO_2$.

2.2. Catalyst characterization

2.2.1. Thermal analysis

Thermogravimetric (TG) and differential thermoanalytical (DTA) studies of dried samples were performed on a Mettler TA 2000C thermoanalyzer in air employing a heating rate of 10 K min^{-1} and α-Al_2O_3 as a reference.

2.2.2. Nitrogen physisorption

The surface areas (S_{BET}), desorption pore volumes (V_P) and desorption average pore diameters ($\bar{d}_P$) were determined by nitrogen physisorption at 77 K using a Micromeritics ASAP 2000 instrument. A cross sectional area of 0.162 nm^2 for the nitrogen molecule was assumed and the pore size distributions were calculated from the desorption branches of the isotherms following the BJH-method [23] in combination with the equation of Halsey [24].

2.2.3. X-ray diffraction

X-ray analysis was carried out on a Siemens D5000 powder diffractometer in a step mode between 10° and 80° 2θ using CuK α radiation. The mean crystallite size of Cu ($\bar{d}_{Cu}$) was calculated from the half-width of the (111) reflection, using the Scherrer equation and assuming spherical crystallites.

2.2.4. Temperature-programmed reduction

The apparatus used for the TPR studies has been described previously [25]. TPR profiles were measured under the following conditions: heating rate 10 K min^{-1}, flow rate 75 cm^3 min^{-1} 5% H_2/Ar.

2.2.5. Nitrous oxide titration

Experiments were carried out using a pulse technique similar to that reported by Evans et al. [26]. Samples were first reduced in flowing H_2/Ar (5% H_2, 75 cm^3 min^{-1}) by heating at 10 K min^{-1} to 473 K. Subsequently the samples were held at this temperature for 30 min and then exposed to a flux of 75 cm^3 min^{-1} of pure hydrogen for 30 min at the same temperature. The hydrogen was purged with 50 cm^3 min^{-1} He at 473 K. After cooling to 363 K under He, pulses of nitrous oxide (0.5 cm^3) were injected. Copper metal surface areas were calculated assuming $1.46 \cdot 10^{19}$ copper atoms per m^2 [26] and an adsorption stoichiometry of $Cu_S/O_{ads} = 2$.

2.3. XPS analysis

X-ray photoelectron spectra were recorded using a Leybold–Heraeus instrument equipped with a high-pressure chamber ($p \leq 1$ MPa), a preparation chamber (10^5–10^{-5} Pa) and an analysis chamber ($\leq 10^{-8}$ Pa). Measurements were carried out at a base pressure of $2 \cdot 10^{-7}$ Pa using MgK α (1253.6 eV) and AlK α (1486.7 eV) radiation, respectively, from a twin anode X-ray source operated at 12 kV voltage and 10 mA current. Two different radiation sources were used to unravel XPS and Auger signal interferences. The 200 mm hemispherical energy analyzer was set to a constant pass energy of 50 eV at an energy scale calibrated versus the $Au4f_{7/2}$ signal at 84.0 eV. Ten scans with an energy step of 100 meV and a step time of 100 ms were recorded for each spectrum. Data acquisition and processing was done by a HP 1000 (model A400) unit using the software package DS100 (Leybold) for spectral deconvolution. Strong charging effects up to 4 eV were observed and binding energies were therefore

corrected by using the $3d_{5/2}$ signal of Zr^{4+} (182.5 eV [27]) as an internal standard.

Three sets of samples, i.e. as prepared (dried, calcined), reduced and after the catalytic reaction of CO_2 and H_2, have been investigated. Reduction was performed by heating the samples in a 1:3 mixture of N_2/H_2 at a pressure of 0.5 MPa with a rate of 6 K min^{-1} to 523 K and holding this temperature for 30 min. The catalytic reaction was performed under the same conditions, except that N_2 was replaced by CO_2.

2.4. Catalytic tests

A continuous tubular fixed-bed micro reactor (8 mm I.D.) operated at 1.7 MPa total pressure was used for catalytic tests. Feed and product gas analysis was performed using a gas chromatograph (Hewlett Packard) equipped with a stainless steel Porapak QS column (5 m, 1/8 inch) and a thermal conductivity detector. For further details of the apparatus refer to Ref. [14].

Standard experiments were carried out using 1.0 g of catalyst under a reactant flow rate of 90 cm^3 (STP) min^{-1} in the temperature range 443–533 K. The reactant gas mixture, containing 25% CO_2 (99.9%) and 75% H_2 (99.999%), was fed from a high pressure cylinder without further purification. Catalysts were reduced prior to activity measurements by heating to 473 K at a rate of 15 K min^{-1} in 1.25% H_2/N_2 at a pressure of 10^5 Pa. The hydrogen concentration was then increased stepwise (30 min per step) in the sequence 2.5/5/10/20/50 to 100%. Activities and selectivities were measured at steady-state after the catalysts had been on stream for 15 h at 493 K. Carbon monoxide, methanol and water were the only products detected.

2.5. FTIR measurements

In situ diffuse reflectance FTIR measurements were carried out on a Bruker IFS 55 FTIR instrument equipped with a diffuse reflectance unit housing a controlled environmental chamber fitted with ZnSe windows (Spectra-Tech) and a nitrogen-cooled MCT detector. For activation the catalysts were heated in a nitrogen/hydrogen mixture up to 523 K with a heating rate of 2 K min^{-1}. Subsequently a background spectrum (R_0) was recorded at 523 K. After switching to a defined reactant flow of 167 ml min^{-1} CO/H_2 or CO_2/H_2, respectively, at a total pressure of 0.6 MPa, DRIFT spectra were recorded with a resolution of 4 cm^{-1} at different time intervals. Depending on the catalyst and the time scale, on which the time dependent changes had to be resolved, 100 to 500 scans were accumulated. DRIFT spectra are presented in the reflectance (R/R_0) mode and not in Kubelka–Munk units, as the black samples absorb strongly across the mid-IR region [28]. For a more detailed description of the experimental setup refer to Ref. [28].

3. Results

3.1. Catalyst characterization

Structural and catalytic properties of the samples, both dried at 403 K and calcined in air at 623 K, are listed in Table 1. Textural characteristics of the catalysts were investigated by nitrogen physisorption. In general, the adsorption/desorption isotherms were of type IV, with a type H4 hysteresis for samples Zr and CrZr and a type H2 hysteresis for sample MnZr according to IUPAC classification [29]. The pore size distributions derived from the desorption branch of the isotherms showed narrow pore size maxima in the range 3.0–3.3 nm for all samples, irrespective of the thermal pretreatment. The observed type H4 hysteresis and the *t*-plots analysis indicated the presence of microporosity for samples Zr and CrZr. Specific mesopore volumes in the range 0.2–0.35 cm^3 g^{-1} were found to slightly decrease, whereas BET surface areas markedly decreased upon calcination at 623 K, resulting in 238 m^2 g^{-1} for Zr and 268 m^2 g^{-1} for CrZr and MnZr (Table 1).

Table 1
Structural and catalytic properties of the samples after drying at 403 K and after calcination at 623 K, respectively

Catalyst	Pretreatment[a] (K)	S_{BET} ($m^2\ g^{-1}$)	V_p[b] ($cm^3\ g^{-1}$)	$\bar{d}_P$[c] (nm)	$\bar{d}_{(Cu)}$[d] (XRD) (nm)	$\bar{d}_{(Cu)}$[d] (N_2O) (nm)	$S_{(Cu)}$[d] (N_2O) ($m^2 g^{-1}$)	T_{max}[e] (K)	Conversion of CO_2[f] (%)	Selectivity to menthol[f] (%)
Cu/ZrO_2	403	353	0.24	3.1	22	12	10.2	498	6.9	70
	623	238	0.23	3.3	19	39	3.1	462/491	4.4	77
$Cu/MnO_x/ZrO_2$	403	392	0.35	3.3	14	15	8.7	486	4.8	58
	623	268	0.29	3.3	15	15	8.6	472	7.3	52
$Cu/CrO_x/ZrO_2$	403	358	0.20	3.0	15	16	8.2	512	4	87
	623	268	0.18	3.1	13	16	8.2	487	4.1	86

[a] Drying under vacuum at 403 K for 15 h; Calcination in air at 623 K for 3 h.
[b] BJH cumulative desorption pore volume.
[c] BJH desorption average pore diameter.
[d] Mean copper crystallite size and copper surface area of the samples after catalytic testing.
[e] Temperature of maximum hydrogen consumption measured by TPR.
[f] Steady state CO_2 conversion and methanol selectivity, respectively, at 493 K and 1.7 MPa after 15 h on stream.

The calcination behavior of the dried materials was monitored by thermoanalytical methods. A broad endothermic event (DTA) between 323 and 443 K, found for all samples, originated from the volatilization of physisorbed and crystalline water, respectively. The corresponding TG curves indicate a total weight loss in the range 10.2–10.8% at 623 K. A narrow exothermic peak perceptible in the DTA curve at higher temperatures is characteristic for the crystallization of initially amorphous zirconia [13,14]. The temperature of this event depended on the sample composition and increased in the order 863 K for Zr, 908 K for CrZr and 933 K for MnZr. Crystallization of amorphous zirconia was verified by XRD.

X-ray analysis of the dried and calcined catalysts, respectively, showed two broad peaks in the range 20 to 40° and 40 to 75° 2θ, indicating the presence of zirconia with a very low degree of crystallinity. Weak characteristic reflections of copper(II)oxide [30] were clearly seen for Zr and CrZr, but not for MnZr. No indication of chromium- or manganese oxides was visible. Subjecting the catalysts to CO_2 hydrogenation conditions after prereduction in hydrogen resulted in metallic copper [31] with mean crystallite sizes ($\bar{d}_{(Cu)}$, Table 1) in the range 12–16 nm for CrZr and MnZr and 19–22 nm for Zr, as estimated from the line broadening of the Cu(111) reflection. The X-ray amorphous state of zirconia was maintained under reaction conditions.

The reduction characteristics of the catalysts are depicted in Fig. 1. TPR profiles of the dried samples exhibit a single reduction peak in the range 486–512 K, indicative for the reduction of copper oxide. Note that no hydrogen consumption due to the reduction of chromium- or manganese oxide was observed for the dried catalysts. Calcination at 623 K caused a slight shift of the T_{max}-values of the reduction profiles to lower temperatures (Table 1) and in significant peak broadening, resulting in two resolved peaks for sample Zr.

3.2. Catalytic behavior in CO_2 hydrogenation

The catalytic performance of the catalysts in CO_2 hydrogenation was investigated after drying at 403 K as well as after calcination in air at 623 K. The temperature dependence of the methanol production rate (r_{MeOH}/mmol s^{-1} kg^{-1}) is shown in Fig. 2. For dried samples, binary copper/zirconia exhibits highest activity for methanol synthesis up to 513 K, followed by CrZr and, least active, MnZr. Copper surface areas (S_{Cu}) measured by N_2O-titration of the

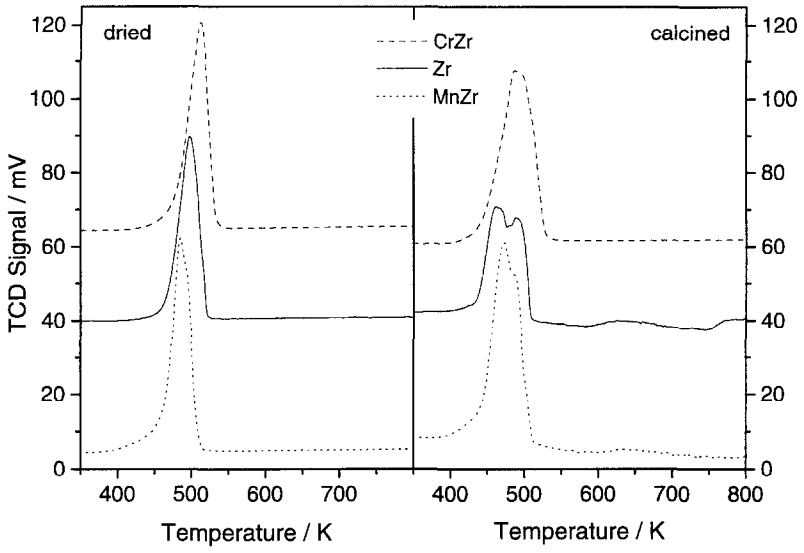

Fig. 1. TPR profiles of catalyst samples after drying at 403 K (left) and after calcination at 623 K in air (right). Conditions of measurement: 75 cm^3/min, 5% H_2/Ar, heating rate 10 K/min.

samples after catalytic testing were highest for Zr and slightly lower for MnZr and CrZr (Table 1). Calcination at 623 K effected a marked decrease in methanol production for Zr, whereas r_{MeOH} remained stable for CrZr and significantly increased for MnZr, thus resulting in similar methanol production rates of the three calcined samples. Note that S_{Cu} of the calcined Zr sample after catalytic testing was markedly lower compared to the dried sample, whereas only a slight decrease was observed for MnZr and CrZr (Table 1). Results for the formation of carbon monoxide, produced via the reverse water gas shift reaction (RWGSR), are presented in Fig. 3. Formation of carbon monoxide (r_{CO}/mmol s^{-1} kg^{-1}) over the dried catalysts is similar for Zr and MnZr, whereas CrZr produces substantially less CO. Calcination effects CO formation similarly as found for methanol production with r_{CO} decreasing for Zr, remain-

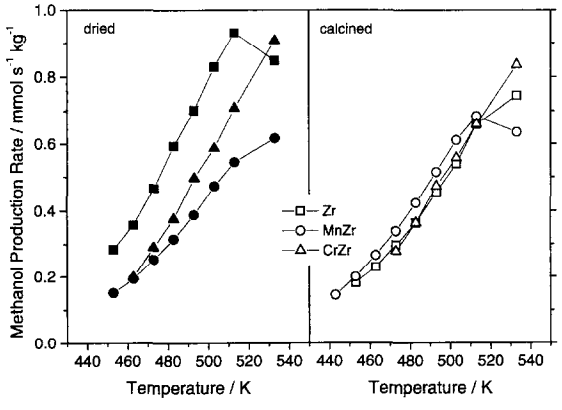

Fig. 2. Carbon dioxide hydrogenation over dried (left) and calcined (right) catalysts. Influence of temperature on methanol production rate (mmol(CH_3OH)/s kg_{cat}). Conditions: 1 g catalyst, 90 cm^3/min, $H_2/CO_2 = 3$, 1.7 MPa.

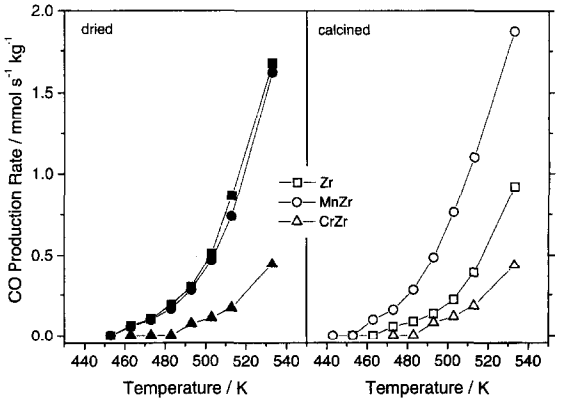

Fig. 3. Carbon dioxide hydrogenation over dried (left) and calcined (right) catalysts. Influence of temperature on carbon monoxide production rate (mmol(CO)/s kg_{cat}). Conditions: 1 g catalyst, 90 cm^3/min, $H_2/CO_2 = 3$, 1.7 MPa.

ing stable for CrZr and increasing for MnZr (Fig. 3). The effect of calcination can also be seen from the CO_2 conversion/methanol selectivity data presented in Table 1. Using CrZr as a catalyst, calcination had no influence on the catalytic behavior. In contrast, CO_2 conversion markedly decreased over Zr and increased over MnZr. Methanol selectivity decreased in the order CrZr > Zr > MnZr, irrespective of sample pretreatment.

3.3. XPS investigation

Representative XP-spectra of the Zr 3d-, C 1s-, O 1s- and Cu 2p-regions are presented in Fig. 4 for sample CrZr after drying at 403 K, after reduction in hydrogen and after CO_2 hydrogenation, respectively. Except for signals due to the promotor components (Cr, Mn), similar characteristics were found for the other catalysts.

The carbon 1s signal consists of two distinct features. The signal at ≈ 289 eV, observed independently of the pretreatment, indicates the presence of carbonate species [32,33], whereas the peak at a binding energy of ≈ 285 eV points to a hydrocarbon contaminant on the catalyst surface. The later signal is drastically reduced after CO_2 hydrogenation (trace C, upper right of Fig. 4). A third peak found at ≈ 281 eV after reduction and after CO_2 hydrogenation, respectively, is due to the presence of a hydrocarbon contaminant on the aluminum sample holder.

The dominant peak at 530.4 eV in the O 1s spectra of the catalyst (lower left spectra in Fig. 4) shows little change upon reduction or catalytic reaction, due to the intense contribution of oxides of zirconium, copper and chromium [33]. A shoulder at lower binding energies indicates the presence of oxygen species on the uncharged aluminium sample holder. The asymmetric component in the O 1s signal at higher binding energies (approximately 532.5 eV) can be attributed to the presence of hydroxyl groups [16,34–36] and/or carbonate species [34,37].

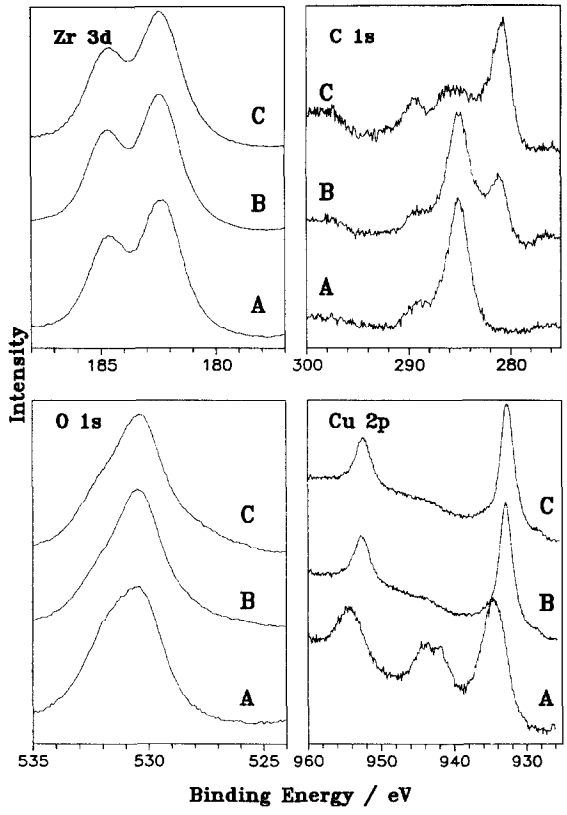

Fig. 4. XP spectra of catalyst CrZr; (A) after drying at 403 K, (B) after reduction with hydrogen at 523 K, and (C) after exposure to CO_2 hydrogenation conditions.

To quantify this effect, the O 1s signal was deconvoluted into two components and the integrated intensities are presented in Table 2. In general, calcination and reduction led to a significant decrease in the surface concentration of the species assigned to carbonate and/or hydroxyl species, whereas CO_2 hydrogenation caused an increase in the surface concentration of these species compared to the reduced samples. This finding is also reflected by the FWHM values of the O 1s peaks shown in Fig. 4. The value decreases from 3.4 eV for the dried sample to 3.0 eV after reduction and then increases again to 3.2 eV upon CO_2-hydrogenation.

The XP-spectra of the Cu 2p level (trace A, lower right of Fig. 4) are characterized by a main peak accompanied by a satellite line. The binding energy of the Cu $2p_{3/2}$ signal at 934.6

Table 2
Relative fractions of surface oxygen species, calculated from XPS O 1s signals

Catalyst	Pretreatment	Main peak[a] /530.4 eV	Shoulder[b] /532.5 eV
Cu/ZrO_2	dried	71	29
	reduced	84	16
	CO_2/H_2	78	22
Cu/ZrO_2	calcined	81	19
	reduced	89	11
	CO_2/H_2	87	13
$Cu/CrO_x/ZrO_2$	dried	64	36
	reduced	76	24
	CO_2/H_2	73	27
$Cu/CrO_x/ZrO_2$	calcined	81	19
	reduced	82	18
	CO_2/H_2	79	21
$Cu/MnO_x/ZrO_2$	dried	75	25
	reduced	80	20
	CO_2/H_2	71	29
$Cu/MnO_x/ZrO_2$	calcined	79	21
	reduced	85	15
	CO_2/H_2	79	21

[a]Assigned to surface oxide species.
[b]Assigned to surface carbonate and/or hydroxyl species.

eV together with the peak half width of 3.8 eV and the characteristic shake-up feature at a binding energy of 944 eV are indicative for Cu^{2+} species [38,39]. After in-situ reduction with hydrogen, the shake up feature disappeared and the binding energy of the Cu $2p_{3/2}$ signal is lowered to 932.7 eV, accompanied by a decrease in the peak half width to 2.1 eV, indicating that Cu^{2+} has been reduced (trace B, lower right of Fig. 4). Changes due to reduction are also reflected in the corresponding Auger spectra (not shown). The Auger value ($E_{kin,\ Auger} + E_{b,2p} \equiv h\nu +$ Auger parameter) between 1850 and 1851.5 eV found for all samples after reduction and after CO_2 hydrogenation suggests that copper exists predominantly in the metallic state (Cu^0) [39].

An inherent problem of XPS measurements of the ternary component (Cr, Mn) of the catalysts investigated resulted from the difficulty in distinguishing between the simultaneous occurrence of different oxidation states. For the dried CrZr catalyst the $2p_{3/2}$ signal of chromium is situated at a binding energy of 577.0 eV and is separated by a multiplet splitting of 9.8 eV from the $2p_{1/2}$ peak. Similar spectra are observed after reduction and catalytic reaction. The binding energy and the spin-orbit splitting are characteristic for Cr(III)-species [37,40–43], although a contribution of Cr(IV) cannot be excluded as the 2p binding energy [41] and the multiplet splitting [43] of Cr^{4+} are close to that of Cr^{3+}. The full width at half maximum (FWHM) of 3.1 eV for the Cr $2p_{1/2}$ peak is in accordance with literature values [40,41], indicating no significant contribution of oxidation states +5 ($E_B = 577.6$ eV) or +6 ($E_B = 579.4$ eV) [43]. A different picture emerges for the calcined sample as can be seen from Fig. 5. The shape as well as the binding energies of the chromium 2p level peaks are different depending on the pretreatment conditions. In the case of the catalyst calcined in air at 623 K (Fig. 5A), the broad chromium $2p_{1/2}/2p_{3/2}$ doublet ($E_B = 588.2/579.4$ eV, $\Delta E = 8.8$ eV) with a

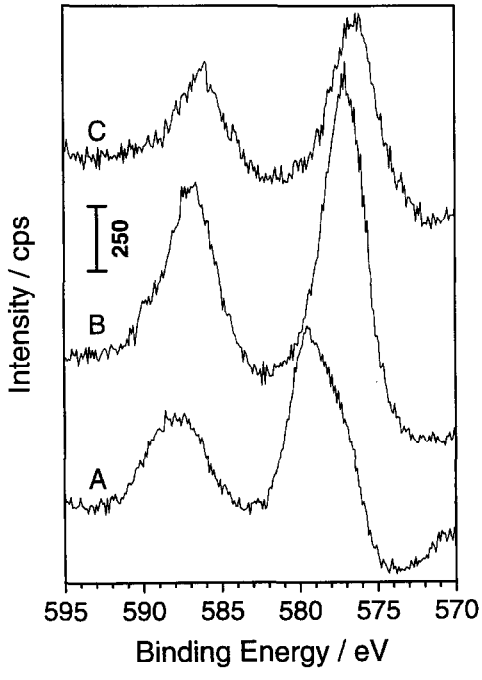

Fig. 5. XP spectra of Cr 2p core level of catalyst CrZr; (A) after calcination in air at 523 K, (B) after reduction with hydrogen at 523 K and (C) after exposure to CO_2 hydrogenation conditions.

FWHM of 4.1 eV for the Cr $2p_{3/2}$ peak is indicative for a superposition of contributions from different oxidation states. The difference is particularly evident if the spectrum is compared with the one of the reduced catalyst (Fig. 5B) and of the sample after reaction with CO_2/H_2 (Fig. 5C), where FWHM values of 3.1 and 3.3 eV, respectively, were found for the Cr $2p_{3/2}$ peak. The coexistence of several oxidation states on the surface of chromia supported on different carrier oxides was occasionally reported [41,43–45] with the contributions depending on the preparation procedure, Cr-loading and pretreatment conditions. For chromia–alumina catalysts containing 5–20 wt% Cr_2O_3, Okamoto et al. [41] observed Cr^{3+} before calcination, whereas a mixture of Cr^{3+} ($E_B = 577.7$ eV, $\Delta E = 9.8$ eV) and Cr^{6+} ($E_B = 579.8$ eV, $\Delta E = 9.0$ eV) was found after calcination at 773 K, as evidenced by a shoulder at the lower binding energy side of the $2p_{3/2}$ peak for Cr(VI). The simultaneous occurrence of Cr(III), Cr(IV), Cr(V) and Cr(VI) surface species was also reported by Köhler et al [44,45] for chromium oxide supported on titania after calcination at 573 K. The existence of ferromagnetic CrO_2 has been proposed from EPR results [44]. Similar mixed valence states have been reported by Cimino et al. [42] for a CrO_x/ZrO_2 catalyst calcined and evacuated at different temperatures. After reduction and CO_2 hydrogenation, respectively, both samples contain predominantly Cr(III) surface species, as indicated by the Cr $2p_{3/2}$ peaks at 577.1 eV (FWHM = 3.1 eV) and 576.4 eV (FWHM = 3.3 eV) and the spin-orbit splitting of 9.8 eV. Sohn and Ryu [37] also reported reduction of Cr(VI) species to Cr(III) with a binding energy of 576.7 eV upon treatment of a calcined CrO_x/ZrO_2 catalyst with H_2.

The Mn 2p-region of the XPS spectra of the MnZr catalyst is presented in Fig. 6 for the dried sample. The binding energy for Mn $2p_{3/2}$ of 642.8 eV (FWHM = 3.8 eV) for the as prepared sample is shifted to 641.7 eV (FWHM = 4.1 eV) upon reduction with hydrogen and CO_2 hydrogenation, respectively. Independent of the pretreatment, the $2p_{3/2}$ and $2p_{1/2}$ peaks are separated by ≈ 11.8 eV. Referring to the values reported in the literature for the Mn $2p_{3/2}$ binding energies (642.2–642.4 eV MnO_2, 641.3–641.8 eV Mn_2O_3, 641.0–641.2 eV Mn_3O_4, 641.3–641.7 eV MnO) [33,46], no clear assignment can be made for the manganese species present on the surface of the catalyst since both Mn^{3+} and Mn^{2+} species have essentially the same binding energies. However, the values observed for the peak half width of the Mn $2p_{3/2}$ features were higher than those reported for pure manganese oxides with a single oxidation state (e.g. 3.3 eV for MnO_2) [46], thus indicating that manganese is present in more than one oxidation state. The occurrence of weak shake-up satellites in the Mn 2p spectra (dashed lines in Fig. 6) indicates that manganese is present in all samples at least partly as Mn^{2+} (MnO or Mn_3O_4) [46]. Several studies have been reported with manganese oxide containing catalysts [46–50]. Koh et al. [50] investi-

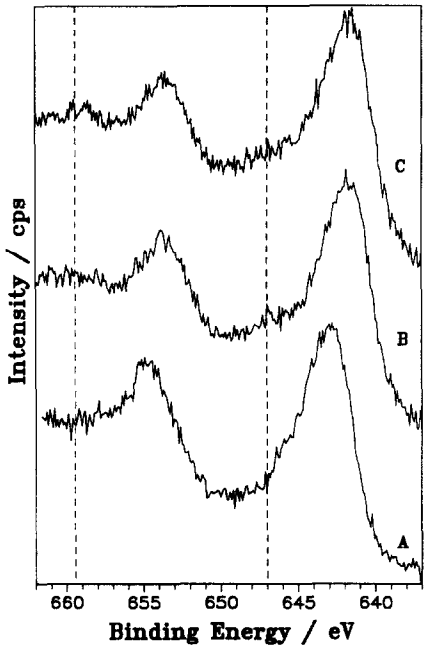

Fig. 6. XP spectra of Mn 2p core level of catalyst MnZr; (A) after drying at 403 K, (B) after reduction with hydrogen at 523 K and (C) after exposure to CO_2 hydrogenation conditions.

gated Mn-Zr oxide catalysts prepared by coprecipitation and found the Mn $2p_{3/2}$ peaks within 641.4 ± 0.4 eV after calcination at 773 K. XRD analysis showed that manganese oxide was composed of a mixture of Mn_3O_4 and Mn_2O_3.

The surface concentrations of the catalyst constituents were estimated from the integrated intensity of the most prominent feature using the standard values given for the instrument [51] and following the procedure outlined in Ref. [52]. Regardless of the composition of the samples and whether the catalysts were dried or calcined, the values presented in Table 3 show some general trends. The surface composition deviates for all samples significantly from the bulk composition, with the surface concentration of zirconium being enhanced relative to copper. Highest Cu/Zr ratios are observed for dried and calcined catalysts, whereas reduction and catalytic testing caused a substantial decrease in the relative surface concentration of copper. For Zr and CrZr calcination had no significant influence on the Cu/Zr ratio after catalytic testing, whereas a distinct increase in the relative surface concentration of copper is observed for MnZr.

Compared to the bulk concentration, the relative surface concentration of the ternary component was markedly lower for the MnZr series and slightly lower for the dried CrZr series. Generally, Mn and Cr surface concentrations are higher for calcined catalysts. Moreover, an increase of the concentration of the ternary component is observed upon reduction and catalytic testing, respectively, for all samples, with the effect being most pronounced for calcined CrZr.

3.4. Adsorbed surface species

Previous IR spectroscopic studies of metal/zirconia catalysts under various reaction conditions [53–57] indicated that the surface species associated with methanol formation appear to be the same, regardless of whether one starts from CO/H_2 or CO_2/H_2; there are, however, pronounced differences with respect to relative concentrations.

Table 3
Relative surface fractions of catalyst components and Cu/Zr ratios, determined from the corresponding XPS peaks

Catalyst	Pretreatment	XPS				
		relative surface concentration/at%				ratio
		Cu	Zr	Cr	Mn	Cu/Zr
Cu/ZrO_2	dried	22.9	77.1	—	—	0.30
	reduced	9.2	90.8	—	—	0.10
	CO_2/H_2	9.9	90.1	—	—	0.11
Cu/ZrO_2	calcined	21.4	78.9	—	—	0.27
	reduced	10.5	89.5	—	—	0.12
	CO_2/H_2	9.9	90.1	—	—	0.11
$Cu/ZrO_2/CrO_x$	dried	18.2	70.8	10.9	—	0.26
	reduced	10.6	77.6	11.8	—	0.14
	CO_2/H_2	11.0	77.6	11.5	—	0.14
$Cu/ZrO_2/CrO_x$	calcined	21.8	66.5	11.6	—	0.33
	reduced	9.7	74.1	16.2	—	0.13
	CO_2/H_2	10.6	73.0	16.4	—	0.15
$Cu/ZrO_2/MnO_x$	dried	21.5	73.6	—	4.9	0.29
	reduced	8.0	84.7	—	7.3	0.09
	CO_2/H_2	8.8	84.1	—	7.1	0.10
$Cu/ZrO_2/MnO_x$	calcined	19.4	75.4	—	5.2	0.26
	reduced	8.9	82.7	—	8.4	0.11
	CO_2/H_2	11.2	81.1	—	7.6	0.14

Fig. 7 depicts the DRIFT spectra in the range 3400–800 cm^{-1} obtained at different time intervals for the dried, reduced CrZr catalyst after switching the nitrogen/hydrogen mixture to a flow of CO_2/H_2 (1:3). Peaks due to surface carbonates (absorptions between 1700 and 1200 cm^{-1} and a broad peak at 1060 cm^{-1}) and surface-bound formates (signals at ≈2880, 1600, 1390 and 1370 cm^{-1}) are immediately observed (upper trace in Fig. 7). The surface concentration of the formate species increases as a function of reaction time during the first 20 min and then levels off, as denoted by the constant intensity of the C–H stretch at 2880 cm^{-1}, suggesting that the adsorption sites for this species become saturated. Gaseous CO (doublet centered at 2144 cm^{-1}) and H_2O (narrow lines in the region of 1400–1800 cm^{-1} due to the roto-vibrational spectrum of H_2O) as products of the reverse water gas shift reaction (RWGSR) are also formed immediately. Subsequent to the rapid formation of carbonate and formate species, two characteristic bands located at 2820 and 1140 cm^{-1} develop (second trace in Fig. 7), which can be assigned to π-bound formaldehyde species [56]. Simultaneously with the appearance of formaldehyde, peaks at 2930, 2820 and 1050 cm^{-1} (second trace in Fig. 7) due to methylate species [56] (CH_3O^-) start to grow. Intensities of both species strongly increase with reaction time. A concomitant decrease of surface carbonates can be deduced from the intensity loss of the bands characteristic for bidentate carbonate at 1550 cm^{-1} and 1310 cm^{-1} [54,58,59]. In a static atmosphere traces of gaseous methane were detectable (spectra not shown).

When starting from CO as a reactant, negative intensities are discernible at 3780 and 3680 cm^{-1}, indicating the consumption of isolated and bridge-bound OH groups on the support [58]. The loss of intensity between 3800 and 3600 cm^{-1} leveled off when no more surface formate was formed (not shown). In addition to the features observed with CO_2/H_2, doubly-bound CO (1960 cm^{-1}) and a small peak at 1445 cm^{-1}, assigned to the δ(CH) mode of surface methylate [60], are detected. Trace amounts of singly surface bound CO are indicated by the asymmetry of the P-branch of the CO gas-phase doublet at ca. 2120/2180 cm^{-1}.

In order to obtain information regarding the differences of the adsorbate coverage on the surface of the working catalysts, FTIR spectra were monitored during CO- and CO_2- hydrogenation. Spectra obtained 105 min after the flow had been switched from N_2/H_2 to CO/H_2 are displayed in Fig. 8 (left panel) for the different dried catalysts. Characteristic differences in the spectra are observed for the negative intensities between 3800 and 3600 cm^{-1}, showing that consumption of surface hydroxyl groups in CO hydrogenation decreases in the order Zr > MnZr > CrZr. Formation of singly-bound CO is strongest on MnZr, as evidenced by the shoulder on the P-branch of the CO gas-phase doublet at ca. 2120/2180 cm^{-1}. In addition doubly-bound CO (1960 cm^{-1}) is ob-

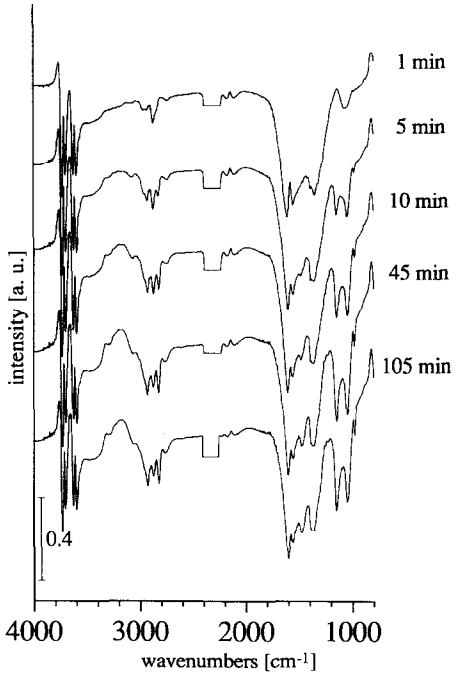

Fig. 7. Development of surface species on catalyst CrZr exposed to a flow of CO_2/H_2 = 1:3. DRIFT spectra with a resolution of 4 cm^{-1} were recorded at 523 K and 0.6 MPa total pressure, subsequent to a step change of the flow from N_2/H_2 to CO_2/H_2.

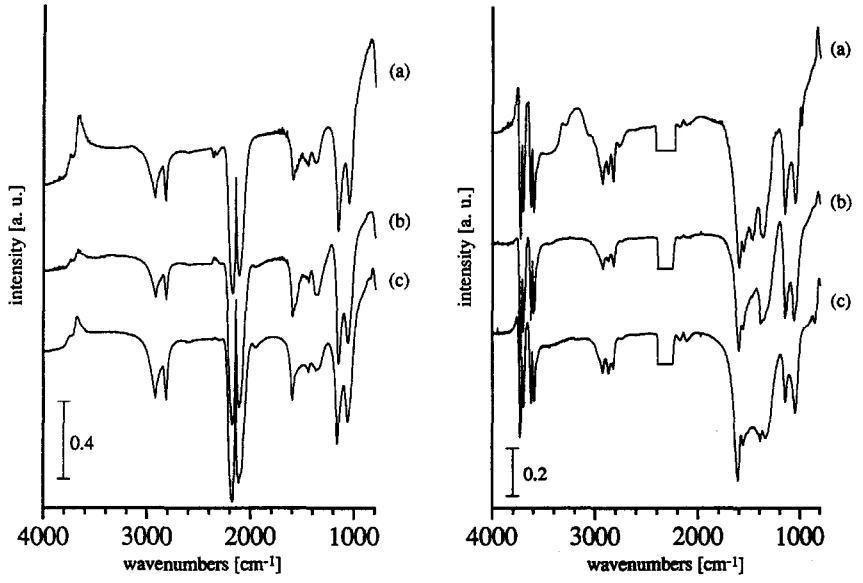

Fig. 8. CO hydrogenation (left) and CO_2 hydrogenation (right) over dried catalyst Zr (A), CrZr (B) and MnZr (C) at 523 K and 0.6 MPa total pressure. DRIFT spectra were recorded 105 min after the flow had been changed from H_2/N_2 to the corresponding reaction mixture.

served for MnZr and CrZr, whereas trace amounts of gaseous CO_2 at 2349 cm^{-1} and of H_2O (multiplet around 1600 cm^{-1}) are detected for Zr. No significant differences are found for surface formate and methylate species and for adsorbed formaldehyde, respectively, with the different catalysts.

When starting from CO_2 as a reactant (Fig. 8, right panel), more carbonate species are formed on the surface of Zr compared to MnZr and CrZr, as indicated by the intensities of the bands between 1700 and 1200 cm^{-1}. Similarly, the surface concentration of formates is highest on the binary copper/zirconia sample, as evidenced by the absorptions at 2960 and 2750 cm^{-1}. These two bands are assigned to combination modes of the asymmetric and symmetric C–O stretch with the δ(C–H) mode of formate and are only detectable for higher surface concentrations [61]. Concerning the formation of π-bound formaldehyde (1140 cm^{-1}) and methylate species (1050 cm^{-1}) similar surface concentrations are found for Zr and CrZr, whereas lower amounts are detected for MnZr. Formation of gas phase CO as a product of the RWGS reaction is comparable for Zr and MnZr and substantially lower for CrZr.

4. Discussion

The comparative activity and selectivity study of CO_2 hydrogenation over CrO_x and MnO_x modified copper/zirconia catalysts reveals marked differences in catalytic performance, which moreover depend on the thermal treatment. Calcination of the dried samples at 623 K substantially decreased CO_2 conversion for binary Cu/ZrO_2, whereas conversion remained constant for CrZr and increased by ca. 50% for MnZr, thus exceeding the initial activity of Cu/ZrO_2. For all catalysts, methanol selectivity is governed by the competition of the simultaneously catalyzed methanol synthesis and the reverse water gas shift (RWGS) reaction. Independent of the pretreatment, CrZr produces only minor amounts of CO and thus exhibits highest selectivity to methanol, whereas MnZr shows pronounced activity for CO formation. Overall production of methanol decreases in the order

Zr > CrZr > MnZr for the dried samples. Calcination results in comparable methanol formation for the different catalysts up to 513 K, whereas CrZr is most active for methanol synthesis at 533 K (Fig. 2).

To elucidate the chemical and structural parameters relevant for the variations in the catalytic behavior, the catalysts have been characterized by several techniques. A similar influence of calcination on BET surface area and porosity is observed. Slightly higher surface areas are found for the ternary catalysts. Thermoanalytical measurements of the catalysts reveal that the crystallization peak of the amorphous zirconia is shifted to higher temperatures for CrZr (908 K) and MnZr (933 K) compared to copper/zirconia (863 K) and pure ZrO_2 (710 K) [13]. The higher stability of the amorphous zirconia for CrZr and MnZr is attributed to the presence of Cr and Mn ions. Koh et al. [50] found that sintering and crystallite growths of zirconium oxide particles can be retarded by the incorporation of Mn. Sohn and Ryu [37] reported that the addition of chromium oxide to zirconia shifted the phase transition of ZrO_2 from amorphous to tetragonal to higher temperatures. They further showed that the zirconia support stabilizes CrO_x in a well dispersed state. Cimino et al. [42] have shown that supported chromium oxide is an effective antisintering agent for zirconia, thus influencing the development of textural properties with temperature in comparison with pure zirconia. The stabilizing effect was suggested to be an indication of a strong interaction with the support.

The third component as well as the thermal treatment significantly influenced copper dispersion. N_2O-titration reveals the highest copper surface area for dried Zr, which also shows highest activity for methanol formation. Calcination causes substantial decrease in the copper surface area for Zr, whereas S_{Cu} is only slightly affected for MnZr and CrZr. Concomitantly, methanol formation decreased substantially for catalyst Zr upon calcination, whereas it was not significantly affected with CrZr and slightly increased with MnZr. Comparing mean copper crystallite sizes estimated from the X-ray line broadening of the Cu (111) reflection with values calculated from copper surface areas by using a half sphere model shows similar copper particle sizes for both methods with MnZr and CrZr, whereas a pronounced discrepancy is observed for catalyst Zr (Table 1). Note that XRD measurements were performed ex situ, i.e. after exposing the catalysts to air, which can results in different degrees of reoxidation of reduced copper and thus in different particle sizes of the remaining metallic Cu. As already mentioned, chromia was occasionally reported to retard thermally induced sintering of copper [16,17,19]. This observation is also reflected by the high methanol synthesis activity of CrZr at 533 K and by the finding that the mean copper crystallite size of the calcined samples used for the TPR experiments (maximum temperature 873 K) increased to 25 nm and 21 nm for Zr and MnZr, respectively, whereas it amounted to only 13 nm for CrZr. XRD showed no indication of a copper chromate phase for the later sample.

XPS measurements allow no direct correlation of the catalytic properties of the samples and the oxidation state of the catalyst components. Copper and zirconium are found in the same oxidation state in all systems. Chromium was mainly present as a Cr^{3+} surface species under reaction conditions for CO_2 hydrogenation, whereas manganese oxide apparently exists as a mixture of Mn_3O_4 and Mn_2O_3. As regards the nature of surface oxygen species XPS revealed the presence of hydroxyl groups [16,34–36] and/or carbonate species [34,37]. FTIR investigations similarly indicated the presence of both hydroxyl groups and carbonate species on the catalyst surface. Consequently, it can be concluded that hydroxyl groups as well as carbonate type species contribute to the O 1s signal at 532.5 eV. For all catalysts XPS showed a lower surface concentration of copper compared to the corresponding bulk composition. Reduction with hydrogen and catalytic testing further decreased the copper surface concentra-

tion, as evidenced by the decreasing Cu/Zr ratios (Table 3). Note that after CO_2 hydrogenation the Cu/Zr ratio was highest for the CuCr catalyst, independently of the thermal treatment and for calcined MnZr. The finding is corroborated by the mean copper crystallite sizes (Table 1), which are lowest for these samples. Regarding the ternary component, reduction increased the surface concentration of both Mn and Cr, with the latter being comparable to the bulk concentration, whereas less Mn was observed on the surface of the catalyst.

The reaction pathway derived from the results of the DRIFT investigation shows that methanol synthesis from CO_2/H_2 starts with rapid formation of surface carbonate and formate species. The concentration of the formate species first increases with reaction time and reaches a steady-state thereafter, suggesting that the adsorption sites for this species become saturated. The formation of formates is paralleled by a loss of surface hydroxyl groups, which ceases at the same time when the formate concentration on the catalyst surface has reached steady state. Therefore we conclude that formates are formed by interaction of carbon oxides with surface hydroxyl groups. The signals between 1700 and 1200 cm^{-1} show that mono- and bidentate carbonate species are present on the catalyst surface during methanol synthesis. Both types of carbonates are formed from CO_2 and surface O^{2-}. Bidentate surface carbonate is reduced to π-bound formaldehyde and water as evidenced by the loss of the signals at 1550 and 1310 cm^{-1}, [58,62] and the concomitant increase of the band at 1140 cm^{-1}. This reaction step involves adsorbed carbon monoxide as an intermediate. Surface-bound formaldehyde is further reduced to surface methylate, which desorbs as methanol after a last reduction step. Note that no clear correlation between the formation of π-bound formaldehyde and methylate and the consumption of surface formates can be observed. The intensities of the latter species become constant after several minutes reaction time, whereas the formation of π-bound formaldehyde and methylate continues over the whole time span of observation. The formation of these two species parallels the formation of gas phase methanol. π-bound formaldehyde is regarded as the pivotal intermediate in methanol synthesis over zirconia based catalysts. Gaseous CO as a product of the reverse water gas shift reaction decreases in the order MnZr > Zr > CrZr, which is in accordance with the activity data for the RWGS reaction. Similarly, the surface concentration of methylate decreases in the order of the methanol activity found in catalytic tests.

5. Conclusions

Addition of chromium- and manganese oxides to copper/zirconia methanol synthesis catalysts results in increased thermal stability of the catalysts. The presence of Mn or Cr suppressed sintering of the copper crystallites and stabilized the amorphous state of zirconia. Calcination at 623 K yielded catalysts which exhibited similar activity for methanol synthesis up to 513 K, whereas CrZr was most active at higher temperatures. CO formation decreased in the order MnZr > Zr > CuCr. This behavior correlates with the observation of most intense DRIFT signals of adsorbed CO on the MnZr catalyst.

No differences in the state of copper and zirconia for the different catalysts were found by XPS. The CrZr sample, which provides highest methanol production rates at high temperatures, exhibits the highest Cu/Zr surface concentration ratio.

The reaction pathway proposed from the observed correlations of surface species as revealed by FTIR spectroscopy is in accordance with a methanol synthesis mechanism in which surface carbonates are reduced via adsorbed CO to π-bonded formaldehyde, surface-bound methylate and finally the methanol product. Formaldehyde and methylate surface concentrations are higher on the Zr and CrZr catalysts that exhibit high methanol selectivities, as com-

pared to MnZr where strong RWGS activity is observed.

Acknowledgements

Financial support by the Deutsche Forschungsgemeinschaft and the Schweizerische Bundesamt für Energiewirtschaft (BEW Projekt EF-REN 93 020) is gratefully acknowledged.

References

[1] K. Klier, Adv. Catal. 31 (1982) 243.
[2] G.C. Chinchen, P.J. Denny, J.R. Jennings, M.S. Spencer, K.C. Waugh, Appl. Catal. 36 (1988) 1.
[3] Y. Amenomiya, Appl. Catal. 30 (1987) 57.
[4] B. Denise, R.P.A. Sneeden, Appl. Catal. 28 (1986) 235.
[5] G.J.J. Bartley, R. Burch, Appl. Catal. 43 (1988) 141.
[6] B. Denise, O. Cherifi, M.M. Bettahar, R.P.A. Sneeden, Appl. Catal. 48 (1989) 365.
[7] D. Gasser, A. Baiker, Appl. Catal. 48 (1989) 279.
[8] G.J. Millar, C.H. Rochester, S. Bailey, K.C. Waugh, J. Chem. Soc. Faraday Trans. 88 (1992) 2085.
[9] G.C. Chinchen, P.J. Denny, D.G. Parker, G.D. Short, D.D. Whan, M.S. Spencer, K.C. Waugh, Am. Chem. Soc. Div. Fuel Chem. 29 (1984) 178.
[10] G.C. Chinchen, K.C. Waugh, D.A. Whan, Appl. Catal. 25 (1986) 101.
[11] G.C. Chinchen, K.C. Waugh, J. Chem. Soc. Faraday Trans. 87 (1986) 3399.
[12] G.C. Chinchen, M.S. Spencer, K.C. Waugh, D.A. Whan, J. Chem. Soc. Faraday Trans. I 83 (1987) 2193.
[13] R.A. Koeppel, A. Baiker, C. Schild, A. Wokaun, Stud. Surf. Sci. Catal. 63 (1990) 283.
[14] R.A. Koeppel, A. Baiker, A. Wokaun, Appl. Catal. A 84 (1992) 77.
[15] A. Baiker, M. Kilo, M. Maciejewski, S. Menzi, A. Wokaun, Stud. Surf. Sci. Catal. 75 (1993) 1257.
[16] J.M. Campos-Martín, A. Guerrero-Ruiz, J.L.G. Fierro, J. Catal. 156 (1995) 208.
[17] C.E. Hofstadt, M. Schneider, O. Bock, K. Kochloefl, Stud. Surf. Sci. Catal. (1983) 709.
[18] W. Kotowski, J. Klimiec, J. Tomaszewska, W. Czelakowski, Chem. Ing. Technol. 55 (1983) 871.
[19] E.M. Calverley, R.B. Anderson, J. Catal. 104 (1987) 434.
[20] J.C. Slaa, J.G. Van Ommen, J.R.H. Ross, Catal. Today 15 (1992) 129.
[21] M. Fujiwara, H. Ando, M. Tanaka, Y. Souma, Bull. Chem. Soc. Jpn. 67 (1994) 546.
[22] H.W. Chen, J.H. Lin, J. Phys. Chem. 96 (1992) 10353.
[23] E.P. Barrett, L.S. Joyner, P.P. Halenda, J. Am. Chem. Soc. 73 (1951) 373.
[24] G. Halsey, J. Chem. Phys. 16 (1948) 931.
[25] R.A. Koeppel, J. Nickl, A. Baiker, Catal. Today 20 (1994) 45.
[26] J.W. Evans, M.S. Wainwright, A.J. Bridgewater, D.J. Young, Appl. Catal. 7 (1983) 75.
[27] M. Kilo, M. Hund, G. Sauer, A. Wokaun, A. Baiker, J. Alloys Compd. 236 (1996) 137.
[28] J. Weigel, R.A. Koeppel, A. Baiker, A. Wokaun, Langmuir 12 (1996) 5319.
[29] K.S.W. Sing, D.H. Everett, R.A.W. Haul, L. Moscou, R.A. Pierotti, J. Rouquérol, T. Siemieniewska, Pure Appl. Chem. 57 (1985) 603.
[30] Joint Committee on Powder Diffraction Standards (Ed.), ASTM powder diffraction file 5-0661, Park Lane, Pennsylvania, 1979.
[31] Joint Committee on Powder Diffraction Standards (Ed.), ASTM powder diffraction file 4-0838, Park Lane, Pennsylvania, 1979.
[32] R. Schlögl, G. Loose, M. Wesemann, A. Baiker, J. Catal. 137 (1992) 139.
[33] C.D. Wagner, W.M. Riggs, L.E. Davis, J.F. Moulder, G.E. Muilenberg, Handbook of X-Ray Photoelectron Spectroscopy, Perkin-Elmer Corporation, Eden Prairie. 1979.
[34] C.D. Wagner, D.A. Zatko, R.H. Raymond, Anal. Chem. 52 (1980) 1445.
[35] A. Baiker, R. Schlögl, E. Armbruster, H.J.J. Günthcrodt, J. Catal. 107 (1987) 221.
[36] A. Wöllner, F. Langa, H. Schmelz, H. Knözinger, H. Appl. Catal. A: 94 (1993) 181.
[37] J.R. Sohn, S.G. Ryu, Langmuir 9 (1993) 126.
[38] R. Bechara, A. Aboukaïs, J.-P. Bonnelle, J. Chem. Soc. Faraday Trans. 89 (1993) 1257.
[39] B.E. Goodby, J.E. Pemberton, Appl. Spectrosc. 42 (1988) 754.
[40] A. Cimino, B.A. De Angelis, A. Luchetti, G. Minelli, J. Catal. 45 (1976) 316.
[41] Y. Okamoto, M. Fuji, T. Imanaka, S. Teranishi, Bull. Chem. Soc. Jpn. 49 (1976) 859.
[42] A. Cimino, D. Cordischi, S. De Rossi, G. Ferraris, D. Gazzoli, V. Indovina, G. Minelli, M. Occhuzzi, M. Valigi, J. Catal. 127 (1991) 744.
[43] U. Scharf, H. Schneider, A. Baiker, A. Wokaun, J. Catal. 145 (1994) 464.
[44] K. Köhler, C.W. Schläpfer, A. Von Zelewsky, J. Nickl, J. Engweiler, A. Baiker, J. Catal. 143 (1993) 201.
[45] K. Köhler, J. Engweiler, H. Viebrock, A. Baiker, Langmuir 11 (1995) 3423.
[46] A. Wöllner, F. Lange, H. Schmelz, H. Knözinger, Appl. Catal. A: 94 (1993) 181.
[47] L.S. Puckhaber, H. Cheung, D.L. Cocke, A. Clearfield, Solid State Ionics 32-33 (1989) 206.
[48] S. Vepřek, D.L. Cocke, S. Kehl, H.R. Oswald, J. Catal. 100 (1986) 250.
[49] J.A. Brown Bourzutschsky, N. Homs, A.T. Bell, J. Catal. 124 (1990) 73.
[50] D.J. Koh, J.S. Chung, Y.G. Kim, J.S. Lee, I. Nam, S.H. Moon, J. Catal. 138 (1992) 630.
[51] Leybold-Heraeus, Bedienerhandbuch DS100, Köln, 1990.
[52] M.P. Seah, Surf. Interface Anal. 2 (1980) 222.

[53] C. Schild, A. Wokaun, A. Baiker, J. Mol. Catal. 63 (1990) 223.
[54] C. Schild, A. Wokaun, A. Baiker, J. Mol. Catal. 63 (1990) 243.
[55] C. Schild, A. Wokaun, A. Baiker, Fres. J. Anal. Chem. 341 (1991) 71.
[56] A. Wokaun, J. Weigel, M. Kilo, A. Baiker, Fres. J. Anal. Chem. 349 (1994) 71.
[57] J. Weigel, C. Fröhlich, A. Baiker, A. Wokaun, Appl. Catal. 140 (1996) 29.
[58] J. Kondo, H. Abe, Y. Sakata, K. Maruya, T. Onishi, J. Chem. Soc. Faraday Trans. 84 (1988) 511.
[59] R.A. Koeppel, A. Baiker, C. Schild, A. Wokaun, J. Chem. Soc. Faraday Trans. 87 (1991) 2821.
[60] G. Herzberg, Molecular Spectra and Molecular Structure, vol. I–II, 1st ed., Van Nostrand, New York, NY, 1945.
[61] J.F. Edwards, G.L. Schrader, J. Phys. Chem. 89 (1985) 782.
[62] J. Kondo, Y. Sakata, K. Domen, K. Maruya, T. Onishi, J. Chem. Soc. Faraday Trans. 86 (1990) 397.